BNL-222485-2021-TECH

EIC-ADD-TN-025

Task Force Report: ESR Linear Lattice Design

D. Marx

December 2021

Electron-Ion Collider Project

Brookhaven National Laboratory

U.S. Department of Energy

USDOE Office of Science (SC), Nuclear Physics (NP) (SC-26)

Notice: This technical note has been authored by employees of Brookhaven Science Associates, LLC under Contract No.DE-SC0012704 with the U.S. Department of Energy. The publisher by accepting the technical note for publication acknowledges that the United States Government retains a non-exclusive, paid-up, irrevocable, world-wide license to publish or reproduce the published form of this technical note, or allow others to do so, for United States Government purposes.

DISCLAIMER

This report was prepared as an account of work sponsored by an agency of the United States Government. Neither the United States Government nor any agency thereof, nor any of their employees, nor any of their contractors, subcontractors, or their employees, makes any warranty, express or implied, or assumes any legal liability or responsibility for the accuracy, completeness, or any third party's use or the results of such use of any information, apparatus, product, or process disclosed, or represents that its use would not infringe privately owned rights. Reference herein to any specific commercial product, process, or service by trade name, trademark, manufacturer, or otherwise, does not necessarily constitute or imply its endorsement, recommendation, or favoring by the United States Government or any agency thereof or its contractors or subcontractors. The views and opinions of authors expressed herein do not necessarily state or reflect those of the United States Government or any agency thereof.

Task Force Report: ESR Linear Lattice Design

D. Marx, C. Montag, J.S. Berg, J. Kewisch, Y. Li, V. Ptitsyn, S. Tepikian, F. Willeke, D. Xu,
Brookhaven National Laboratory
G.H. Hoffstaetter, D. Sagan, M. Signorelli, Cornell University
V. Morozov, Oak Ridge National Laboratory
Y. Cai, Y. Nosochkov, SLAC National Accelerator Laboratory
B.R.P. Gamage, Thomas Jefferson National Accelerator Facility

December 9, 2021

Abstract

A new layout and optics for the ESR have been produced with revised spin rotators in IRs 6 and 8, a redesign of IR10, and a new geometric layout for the ring. In this report, the efforts to produce this lattice are documented, including the motivation for design decisions. This new lattice, version 5.5, will be used as the baseline for future studies.

1 Introduction

The Electron Storage Ring (ESR) [1] is being designed to provide longitudinally polarized electron beams at energies of 5, 10 and 18 GeV for collisions with hadrons (protons to heavy ions). The ring consists of six sextants separated by six insertion regions, which are labelled according to the hour markings of a clock from IR2 to IR12. Collisions will occur at IR6, and the possibility of including a second collision point at IR8 is left open as an option for a future upgrade. For the purposes of the current studies, the optics of IR8 is set to replicate IR6 as closely as possible, although there are important geometrical differences.

Achieving high longitudinal polarization of colliding beams is essential for the physics program. The stable spin direction is vertical in the arcs, which means spin rotators are needed around the interaction point (IP) to rotate the spin direction from vertical to longitudinal and vice versa. There are many constraints within the IR, which, taken together, make this a very challenging section to design and match. The goal of this task force was to produce a new version of the ESR lattice with redesigned straight sections IR6 and IR8, including the spin-rotator modules.

2 Spin-rotator configuration

The aim of the spin rotators is to rotate the spin from the vertical direction in the arcs to the longitudinal direction at the IPs. The spin rotators are solenoid-based [2–4] to avoid the excessively large aperture required to accommodate orbit excursions in a pure dipole spin rotator. In general, the spin precesses around an axis parallel to the field direction, namely vertical in dipoles and longitudinal in solenoids, as shown in Fig. 1. A solenoid followed by dipoles can therefore rotate the spin direction from vertical in the arc to radial after the solenoid, and finally

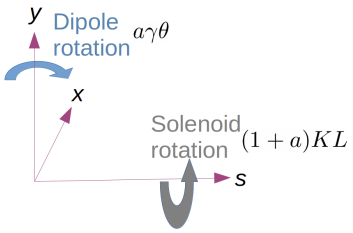


Figure 1: A horizontal dipole of bend angle θ rotates the spin about the vertical axis by $a\gamma\theta$ relative to the reference orbit, where $a = 0.00115965218$ is the anomalous magnetic moment of the electron and γ is the Lorentz factor. A solenoid of length L and strength $K = B_s/(B\rho)$, where B_s is the magnetic field and $(B\rho)$ is the magnetic rigidity, rotates the spin about the longitudinal axis by $(1 + a)KL$.

to longitudinal after the dipoles. The configuration is mirror symmetric about the IP to rotate the spin from longitudinal back to vertical on the other side.

As the spin configuration needs to rotate the spin at three different energies and the dipole angles cannot be changed in operation, the solenoid-bend structure is repeated, as shown in Fig. 2, which offers the required flexibility. However, both the length of the solenoids and the configuration of the dipoles are different in the two cases to optimize to the requirements at various energies and other constraints.



Figure 2: The spin rotators are composed of short- and long-solenoid modules, as well as bend modules, to rotate the spin from vertical in the arcs to longitudinal at the IP and back to vertical on the other side.

Furthermore, each solenoid is actually split into two halves with a set of quadrupoles in between. This unit, collectively called a solenoid module, is shown in Fig. 3. This configuration allows decoupling between the horizontal and vertical planes, as well as horizontal spin-matching conditions, to be fulfilled. There are four half-solenoids per spin rotator: two long and two short. The solenoids are superconducting with a maximum field strength assumed to be 12 T, which is within the comfort zone of Nb_3Sn technology. The quadrupoles must be normal-conducting due to the synchrotron radiation from the solenoids. An alternative scheme involving skew quadrupoles outside of the half-solenoids was also considered and determined to be less desirable due to the

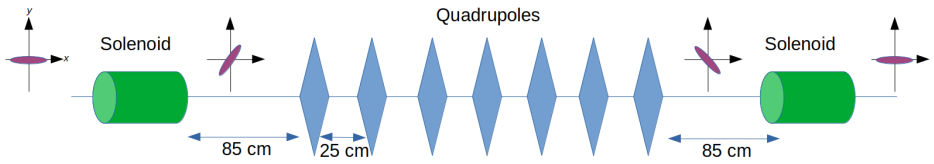


Figure 3: Each solenoid module consists of two half-solenoids with several quadrupoles in between (the number shown is illustrative). By matching the quadrupoles, decoupling between the horizontal and vertical planes can be achieved, as illustrated in the schematic, as well as horizontal spin-matching conditions.

added complexity in dealing with coupling from these skew quadrupoles.

The short-solenoid module sits directly next to the arc with two quadrupoles for matching in between. Between the short- and long-solenoid modules is a bending section consisting of dipoles and quadrupoles for matching. The long-solenoid module leads onto the IR section, containing quadrupoles and dipoles for matching various constraints, including a fixed dipole angle to the IP to complete the spin rotation. The configuration of the spin rotator is as follows: Arc $\rightarrow$ Short-solenoid module $\rightarrow$ Bend module $\rightarrow$ Long-solenoid module $\rightarrow$ IR $\rightarrow$ Long-solenoid module $\rightarrow$ Bend module $\rightarrow$ Short-solenoid module $\rightarrow$ Arc.

There are a number of constraints that need to be met while designing the spin rotators, which are shown in Table 1. Fulfilling all these constraints is a challenging task.

Table 1: Constraints for the solenoid modules.

Constraint	**Motivation**
Matching transfer matrix	Decoupling and horizontal spin matching
Zero (or low) dispersion in solenoids	Dynamic and physical aperture
Short length of solenoid modules	Geometric fit into the IR
Quad length $\geq 0.2\,\mathrm{m}$; separation $\geq 0.25\,\mathrm{m}$	Technical limitations
Quad pole-tip fields $< 0.9\,\mathrm{T}$	Normal-conducting quads
Solenoid fields $< 12\,\mathrm{T}$	Within comfort zone for Nb_3Sn
$0.85\,\mathrm{m}$ drift next to solenoids	Space for warm-to-cold transition, correctors and diagnostics

3 Dispersion suppressor

Ideally we would have zero dispersion in both short- and long-solenoid modules by suppressing the dispersion at the end of the arcs. Various schemes for a dispersion suppressor were studied, including a single missing dipole, two missing dipoles, and only varying quadrupole strengths. The challenge is matching dispersion in as few arc cells as possible, which is necessary because changes in the β and dispersion functions will ruin the sextupole pairing. Previous studies showed that pairing the sextupoles is particularly important for maximizing the dynamic aperture of the 90° lattice. The problem is that there are exactly 16 arc cells and 32 sextupoles in arc 7. Changing the optics of even just the last half-cell would mean that we lose eight sextupoles if we wish to retain the same pairing, which would make the remaining sextupoles much stronger – this is exactly the arc where the sextupole strengths are already very strong. For this reason the preferred solution was to leave the 90° arcs unchanged to the end and to bring the dispersion down in the short-solenoid module and bend module. The dispersion is then zero in the long-solenoid module. The implication of this scheme is that the short solenoids had to be turned off at top energy, which does not allow full longitudinal spin matching.

At intermediate energy of around 10 GeV and lower, the phase advance of the arc FODO cells is 60°, and the short solenoids must be turned on. It would require very large strengths to match the dispersion and its derivative to zero by varying only two quadrupoles, although it can be done with reasonable strengths if all quadrupoles in the last two arc cells are used. As a compromise, it was decided to vary only the quadrupoles in the last arc cell, which is sufficient to lower the dispersion to less than about $0.2\,\mathrm{m}$ in the short-solenoid module. The bend section between the solenoid modules can then be used to bring down the dispersion to zero in the long-solenoid module.

4 Polarization

The exact energies of the working points are chosen such that the spin tune, $a\gamma$, is a half-integer value to keep it as far from an integer as possible. Here, $a = 0.00115965218$ is the anomalous

Table 2: Values of the energy chosen to achieve half-integer values of $a\gamma$. An alternative minimum energy of about 6 GeV is considered for the current study, although the baseline calls for an energy of 5 GeV.

Energy (GeV)	$a\gamma$
17.846	40.5
9.915	22.5
5.949	13.5
5.067	11.5

magnetic moment of the electron and γ is the Lorentz factor. That means that the energies are shifted slightly from their integer values, as shown in Table 2.

The spin rotators must rotate the electron spin from vertical in the arcs to longitudinal at the IP. Let θ_1 and θ_2 represent the bend angles of the bend modules between the short- and long-solenoid modules and between the long-solenoid module and IP respectively. The resulting spin rotations from these bends, relative to the reference orbit, are then

$$\psi_1 = a\gamma\theta_1 \tag{1}$$
$$\psi_2 = a\gamma\theta_2. \tag{2}$$

As the short solenoids are turned off at top energy, the long-solenoid module must rotate the vertical spin by $\pi/2$ into the radial direction. The dipoles between the long-solenoid module and the IP must then rotate the spin by $\pi/2$ into the longitudinal direction, which fixes θ_2.

When both short- and long-solenoid modules are used, there are multiple choices for the bend angles that lead to the desired polarization direction. The solenoid rotation angles are chosen so that the matrix

$$\mathbf{T} = \mathbf{R}_y(\psi_2)\mathbf{R}_z(\phi_2)\mathbf{R}_y(\psi_1)\mathbf{R}_z(\phi_1) \tag{3}$$

rotates the spin vector from pointing along the y-axis into $\pm z$, where $\mathbf{R}_y(\psi)$ is a rotation about the y-axis by angle ψ, which occurs in the dipoles, and $\mathbf{R}_z(\phi)$ is a rotation about the z-axis by angle ϕ, which occurs in the solenoid modules. This condition may be expressed as

$$T_{12} = T_{22} = 0 \tag{4}$$
$$T_{32} = \pm 1. \tag{5}$$

The relations between the spin-rotation angles in the solenoids and dipoles are then:

$$\begin{aligned}
\sin(\phi_1) &= \pm\frac{\cos(\psi_2)}{\sin(\psi_1)} \\
\cos(\phi_1) &= \sin(\psi_2)\sqrt{1-\cot^2(\psi_1)\cot^2(\psi_2)} \\
\sin(\phi_2) &= \pm\sqrt{1-\cot^2(\psi_1)\cot^2(\psi_2)} \\
\cos(\phi_2) &= \cot(\psi_1)\cot(\psi_2).
\end{aligned} \tag{6}$$

The spin-rotation angle in a solenoid is related to the beam-rotation angle by $(1 + a)$, so $\phi = (1 + a)K_s 2L$, where L is the length of a half-solenoid and K_s is its strength. The factor of two arises because there are two half-solenoids in a solenoid module that contribute to the spin rotation. Figure 4 shows the range of polarization given by these equations, where the white blocks represent values of ψ_1 and ψ_2 within which there are solutions to these equations. The red line shows the equation $\theta_1 = 2\theta_2$, which describes the current configuration, although other configurations are also possible. Previously, it had been decided to impose this relation because it provides the largest continuous energy range for polarization ($\theta_2 = 2\theta_1$ provides an equivalent range but results in larger solenoid fields). Fulfilling this condition results in a minimum energy for spin rotation of 5.949 GeV, i.e. one-third of the top energy. At this energy the long solenoid is turned off, and the bend angle that rotates the spin is given by $(\theta_1 + \theta_2)$, so the total bend angle determines the minimum energy. This bend angle and minimum energy is the same as the

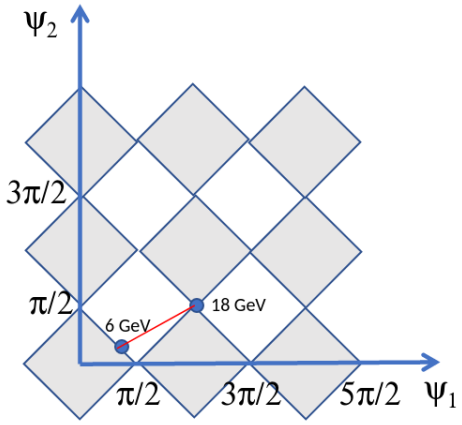


Figure 4: Range of polarization given by Eq. (6), where the white blocks represent values of ψ_1 and ψ_2 within which there are solutions to these equations. The red line shows the solution currently implemented.

previous solution for legacy reasons, although the motivation for choosing this in the previous solution was to achieve the best off-momentum spin-matching, which we have anyway decided to abandon. Setting the minimum energy to the nominal value of 5 GeV would require more extensive geometry changes, i.e. increasing the bend angle between the solenoid modules from 77.57 to 97.81 mrad. This would involve either removing a dipole from the last arc cell and adding the bend angle to the bend module between the solenoid modules, or decreasing the dipole bend angle in the arc cells with a corresponding decrease in the dipole length. In order to find a solution that could be tested in the minimum amount of time, it was decided to postpone studies for 5 GeV to a further iteration, dependent on the success of the current solution in achieving sufficient dynamic aperture and polarization.

The resulting configuration has $\theta_1 = 77.57\,\text{mrad}$ and $\theta_2 = 38.79\,\text{mrad}$. The solenoid spin-rotation angles are given in Table 3.

Table 3: Solenoid spin-rotation angles at various energies, $\phi = (1+a)K_s 2L$, where L is the length of a half-solenoid and K_s is its strength.

Energy (GeV)	ϕ_1 (rad)	ϕ_2 (rad)
17.846	0	$\pi/2$
9.915	0.7111	1.7193
5.949	$\pi/2$	0

5 Matching the solenoid modules

One of the greatest challenges is to match the solenoid modules, consisting of two half-solenoids and quadrupoles. The required conditions on the transfer matrix, M, from the beginning of the first half-solenoid to the end of the second half-solenoid are:

- Symplectic matrix: $M_{11}M_{22} - M_{12}M_{21} = 1$ and $M_{33}M_{44} - M_{34}M_{43} = 1$;
- Decoupled matrix: Block-diagonal form;
- Horizontal spin-matching.

The matrix fulfills the symplectic condition automatically, as it is obtained from symplectic transfer matrices of solenoids, quadrupoles and drifts. The entire transfer matrix can be written as

$$\mathbf{M} = \mathbf{R} \begin{pmatrix} \mathbf{A} & \mathbf{0} \\ \mathbf{0} & \mathbf{B} \end{pmatrix} \mathbf{R}, \tag{7}$$

where $\mathbf{R}$ is the 4-by-4 solenoid rotation transfer matrix and $\mathbf{A}$ and $\mathbf{B}$ are 2-by-2 symplectic matrices. It can be shown [5] that for the transfer matrix to be block diagonal, it is necessary and sufficient that

$$\mathbf{M} = \begin{pmatrix} \mathbf{A} & \mathbf{0} \\ \mathbf{0} & \mathbf{-A} \end{pmatrix}, \tag{8}$$

This condition can be satisfied by three quadrupoles (assuming the symplectic condition holds), and the matrix elements of $\mathbf{A}$ could be brought to any desired values with six quadrupoles.

The horizontal spin-matching conditions for a solenoid module, assuming vertical spin at the entrance, are

$$M_{11} \frac{K_\mathrm{s}}{2} \sin\phi + M_{21} \cos\phi = 0 \tag{9}$$

$$M_{12} \frac{K_\mathrm{s}}{2} \sin\phi + M_{22} \cos\phi + 1 = 0, \tag{10}$$

where $K_\mathrm{s} = B_\mathrm{s}/(B\rho)$ is the solenoid strength, and the spin-rotation angle for a solenoid module is $\phi = (1 + \mathrm{a})K_s 2L$, with L the length of a half-solenoid. Using the symplectic condition, one obtains

$$M_{11} = -\cos\phi \tag{11}$$

$$M_{21} = \frac{K_s}{2} \sin\phi. \tag{12}$$

For $\phi = \pi/2$ the matrix is

$$\mathbf{A} = \begin{pmatrix} 0 & -\frac{2}{K_s} \\ \frac{K_s}{2} & M_{22} \end{pmatrix}, \tag{13}$$

where M_{22} is a free parameter.

Assuming vertical spin at the exit of the solenoid module, i.e. for the downstream module, one obtains the conditions

$$M_{22} = -\cos\phi \tag{14}$$

$$M_{21} = \frac{K_s}{2} \sin\phi, \tag{15}$$

and the matrix is

$$\mathbf{A} = \begin{pmatrix} M_{11} & -\frac{2}{K_s} \\ \frac{K_s}{2} & 0 \end{pmatrix}, \tag{16}$$

where M_{11} is a free parameter.

The above conditions provide five constraints on $\mathbf{M}$ if we take into account the decoupled form, which can be satisfied with five quadrupoles. These conditions were derived making the approximation $(1+a) \approx 1$. If we include terms proportional to a, we can obtain an exact solution for the horizontal spin match; however, this has not yet been implemented in the lattice, and it is still unclear how much this helps increase the depolarization time.

It is possible to form a transfer matrix that works for any incoming spin direction:

$$\mathbf{M} = \begin{pmatrix} -\cos\phi & -\frac{2}{K_\mathrm{s}} \sin\phi & 0 & 0 \\ \frac{K_\mathrm{s}}{2} \sin\phi & -\cos\phi & 0 & 0 \\ 0 & 0 & \cos\phi & \frac{2}{K_\mathrm{s}} \sin\phi \\ 0 & 0 & -\frac{K_\mathrm{s}}{2} \sin\phi & \cos\phi \end{pmatrix}. \tag{17}$$

It can be seen that this matrix fulfills the conditions above. Although matching all solenoid modules to this matrix is valid, it was found that relaxing the constraints by using only those that are strictly necessary (as detailed above) made the match easier. This matrix was still used

for matching the long-solenoid module at 10 GeV, for which the incoming spin direction is not vertical.

As mentioned above, the decision to use only the long solenoids at top energy means that it is not possible to achieve off-momentum spin matching. Studies indicated that this off-momenutum spin matching is not necessary and sacrificing it only decreases the depolarization time by about five minutes (to approximately 24 min). The combined depolarization is in fact dominated by the Sokolov-Ternov time rather than stochastic photon emission, so spin matching does not make a large difference. There is also no spin matching in the vertical plane because of the small beam size in that plane compared to the horizontal.

In addition to matching to this transfer matrix, the solenoid modules must be kept as short as possible. This results in a smaller beamline displacement in both the longitudinal axis and also the horizontal. Larger displacements make matching the IR section to the IP more difficult. In particular, horizontal displacement can require extra dipole chicanes to resolve, which greatly complicate the IR design. For this reason, achieving the minimal length of the short-solenoid module is the most critical. An additional constraint is that the pole-tip fields of the quadrupoles must be kept well below an absolute maximum of 0.9 T. The beam pipe should be round with a constant aperture within each module and satisfy the beam stay-clear requirements. Furthermore, sufficient space must be left for correctors and beam-position monitors (BPMs), as well as the cold-to-warm transitions around the solenoids. As a result, an 85 cm drift space on each side of each solenoid has been included, which should be sufficient for a cold-to-warm transition, a dual-plane corrector, and one or two BPMs.

A multi-objective genetic optimizer was used to match the strengths and lengths of each solenoid module. The long-solenoid module was matched at top energy (17.846 GeV), and the short-solenoid module was matched at 9.915 GeV, as the latter is turned off at top energy. The two objectives were the total length of the solenoid module and the maximum strength of the quadrupoles. Once a satisfactory solution was found, the strengths and positions of the magnets were integrated into the lattice without further changes. For other energies, the strengths needed to be rematched in order to satisfy the different spin-matching conditions. The quadrupoles outside of the module were used to match into the module. The current solution has quadrupoles in the solenoid modules of differing length, which is not optimal due to the increased design and production costs. An alternative solution with same-length quadrupoles resulted in longer solenoid modules, which made matching the IR problematic. Finding a solution that employs fewer unique types of quadrupoles would be beneficial and may be studied further in the future.

6 Matching the dipole-bend section

The dipole-bend section is located between the two solenoid modules. The total bending angle is fixed, and there are matching constraints for the dispersion, which must be brought down to zero in the long-solenoid modules, and β functions, which should be kept below the limit imposed by a pipe-aperture size to constrain the required pole-tip fields. The current solution consists of five dipoles with quadrupoles between each.

7 Matching the IR

The interaction region layout must create a crossing angle between the HSR and ESR lines, create the desired optics functions at the IP, avoid interference with other beamlines and tunnel walls, leave sufficient space for the detectors, leave space for crab cavities and create the desired lattice functions at them, and match to the remainder of the machine.

The sides of the IPs are generally referred to as "forward" and "rear." Geometrically, it is the same side for both the HSR and the ESR. The forward side is the side of the IP that the hadrons are going toward and the side that the electrons are coming from.

IP6 is located 81 cm away from the RHIC IP, toward the center of RHIC. A 25 mrad crossing angle is created by tilting the lines in the horizontal plane by -17 mrad for the HSR and 8 mrad for the ESR, with the HSR further from the RHIC center than the ESR on the forward side. IP8 is located 85 cm from the RHIC IP, toward the center of RHIC. The present studies concluded

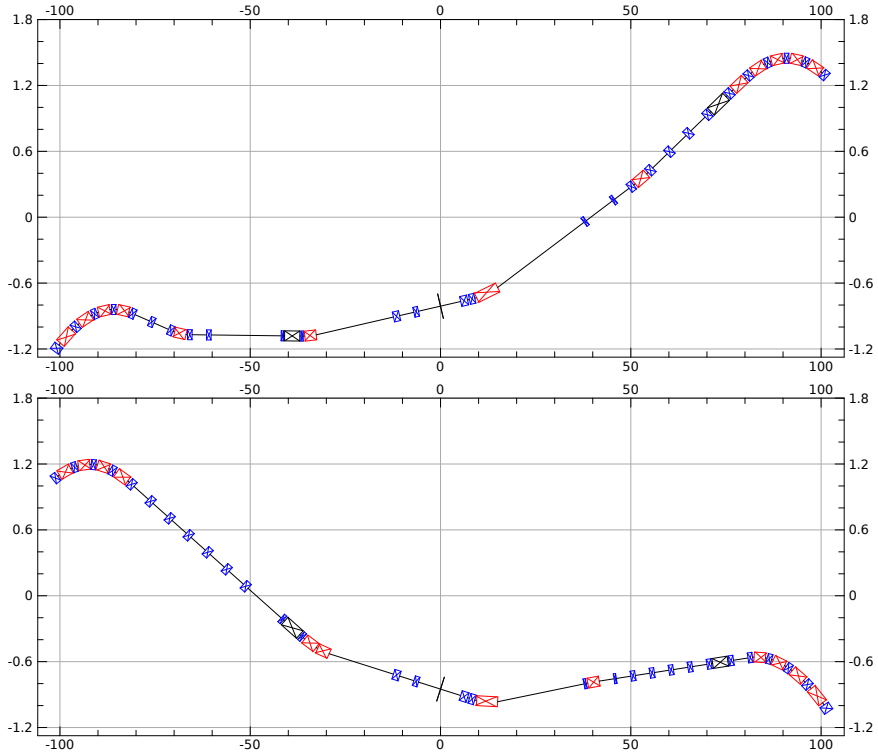


Figure 5: Floor layout of the ESR near IP6 (top) and IP8 (bottom), relative to RHIC's IPs. Magnets shown are from the end of one long spin-rotator solenoid to the beginning of the next. The beam travels from left to right. The longitudinal position is shown on the horizontal axis, and the transverse position is shown on the vertical axis. Both axes are with respect to the current location of the IPs in the RHIC tunnel. Quadrupoles are shown in blue, dipoles in red, and crab cavities in black.

that the horizontal tilt angle for the ESR at IP8 should be -11 mrad (the total crossing angle is 35 mrad at this IP). The ESR horizontal tilt angle is created by adjusting the strengths of the four superbend dipoles at the ends of the arcs. The current floor layout is shown in Fig. 5

The matching sections between the IP and the rotator use the same dipoles used between the spin rotator solenoids (at identical or lower fields), arc quadrupoles (double length in some instances), and large aperture quadrupoles near the crab cavities.

For the ESR,

- β_x and β_y at the IP should have the values given in Table 4
- α_x, α_y, D_x, and D'_x should be zero at the IP
- The horizontal phase advance between the cavities is 360° so the crabbing is confined to

Table 4: ESR β parameters at the IP for the high-divergence configuration, from the CDR.

Proton Energy (GeV)	275	275	100	100	41
Electron Energy (GeV)	18	10	10	5	5
β_x at IP (cm)	59.0	45.0	96.0	78.0	196.0
β_y at IP (cm)	5.7	5.6	12.0	7.1	21.0

the region between the crab cavities. The forward side crab cavity has a phase advance just above 90°. Having both cavities with horizontal phase advance of 90° to the IP is not feasible since it would require large beta functions at the cavities and thereby create issues with transverse collective instabilities. The forward side crab is chosen to be the one closer to the IP because placing it close to the rotator would interfere with the polarimeter in that region.

- At 18 GeV, $\beta_x = 150$ m at the center of the forward crab cavity because that is the largest tolerable value for collective instabilities, and we want to keep the horizontal phase advance between that cavity and the IP as close to 90° as possible. $\beta_x = 100$ m at the center of the rear crab cavity because that beta function is the smallest value sufficient to provide full crabbing with the available voltage.
- $\alpha_x = 0$ at the centers of the crab cavities.
- The rear spectrometer dipole (near the IP) should bend by 18.1 mrad. Small differences from that angle (say a small change in the last significant digit) are tolerable.
- Dipoles should not be placed immediately upstream of crab cavities to avoid radiation hitting the cavities.
- The longitudinal positions of the forward crab cavities should remain unchanged. They are placed to avoid conflicts with detector hardware and the hadron crab cavities.
- The first magnet beyond the spectrometer dipole on the rear side cannot move closer to the IP to avoid interference with detector hardware.
- Achievable field strengths for the quadrupoles.

8 Fitting the ring geometry

The overall geometry of the ESR had to be fitted to meet a number of constraints:

- The beamline must be at least 0.44 m from tunnel wall
- The beamline should not be too close to the HSR, and there should be enough space between them to allow for an access route
- The beamline must cross the HSR at appropriate places
- The total path length is fixed, as is the path length between IP6 and IP8
- The horizontal tilt angles at IP6 and IP8 are set to 8 mrad and 11 mrad respectively
- The arcs near IR6 and IR8 should be as far to the inside as possible

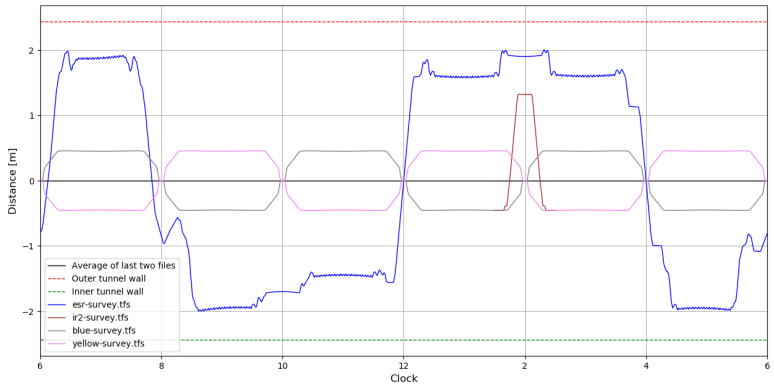


Figure 6: Geometry of the ring with respect to the tunnel center. The ESR is shown alongside the blue and yellow RHIC rings. The HSR layout will closely follow the yellow ring with some deviations, for example at IR2 where the updated layout is shown.

There are a number of significant changes with respect to previous versions of the lattice. The IR8 horizontal tilt angle was varied in an iterative process to optimize the IR layout. The optimized geometry is shown in Fig. 6. The physical layout of the rings will need a detailed integration study.

9 Matching the ring optics

The final step was to match the optics of the complete ring. The arc-cell quadrupole strengths are set to provide 90° phase advance in both planes at top energy. Although the spin rotators and IRs had been matched as individual sections, these had to be matched to the boundary conditions provided by the arc cells. Scripts were written in MAD-X for this matching. Although there were no problems with matching three of the four spin rotators, the rotator on the rear side of IR8 proved tricky to match. A solution was found with slightly larger β-functions. It is not yet known

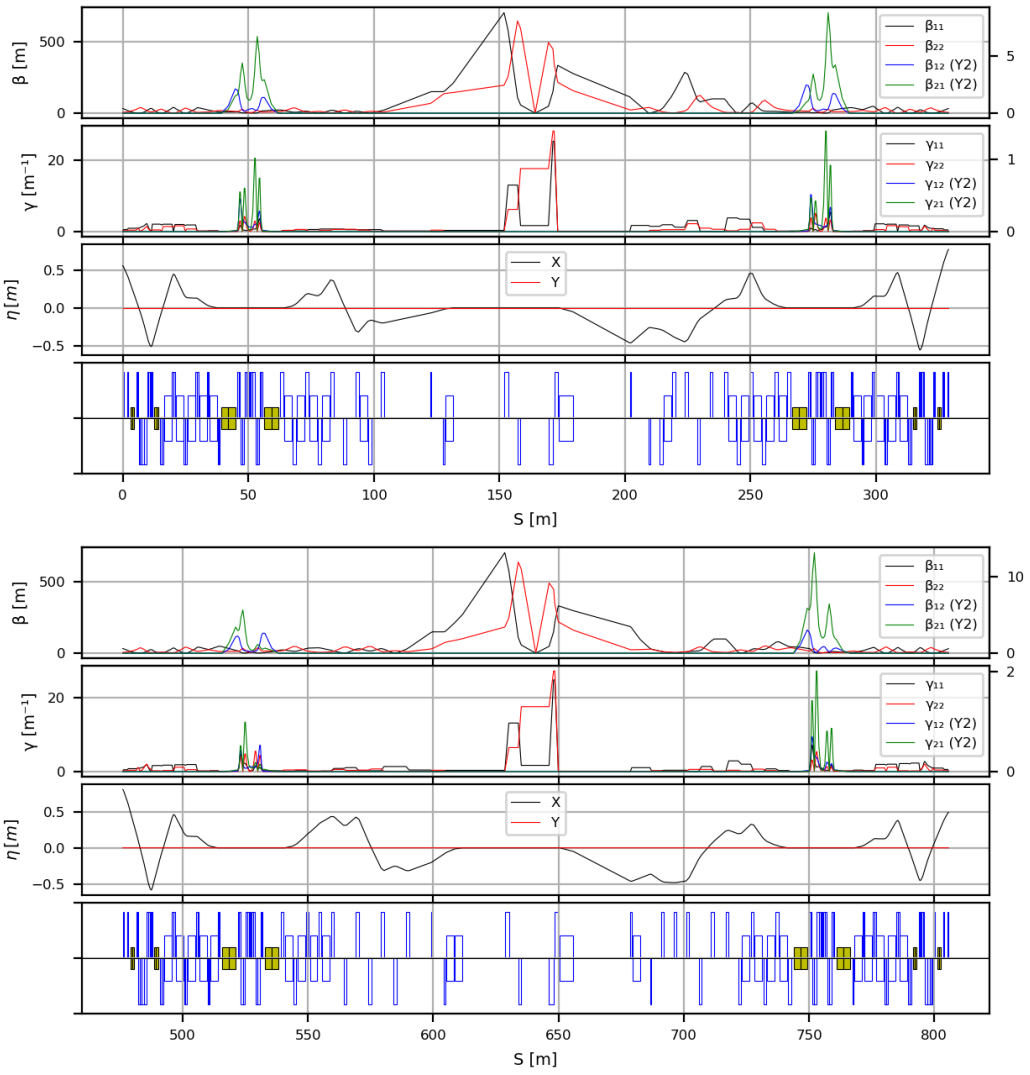


Figure 7: Layout and optics for IR6 (top) and IR8 (bottom), shown from the ends of the neighboring arcs. IR8 is shown for the squeezed case. The beam travels from left to right. The solenoids are shown in yellow.

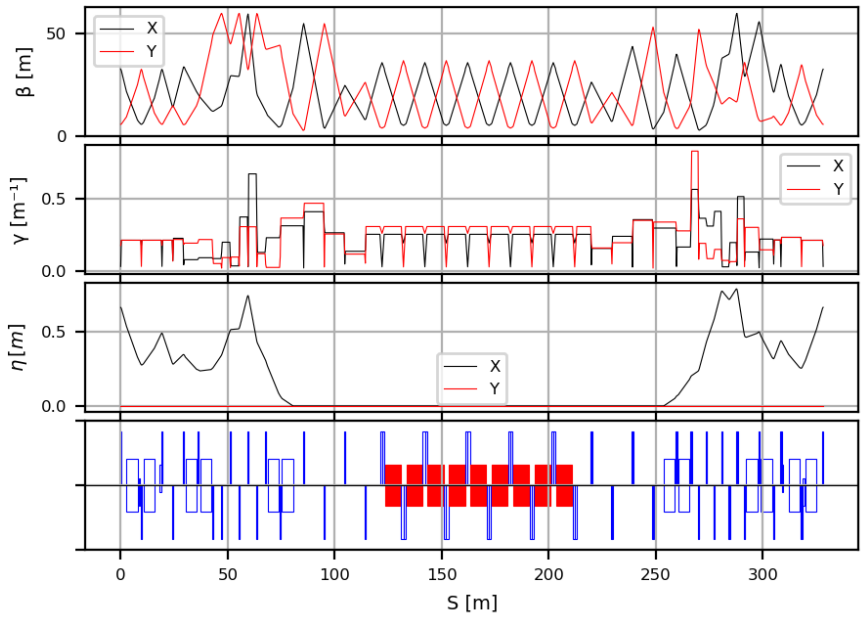


Figure 8: Layout and optics functions for IR10. The RF cryomodules are shown in red.

why this rotator was causing issues given the strong similarities between the rotators, and it is likely that a better match could be found with more extensive changes to quadrupole strengths. Figure 7 shows the layout and optics for IRs 6 and 8.

A redesigned IR10 was inserted assuming nine cryomodules, each 7.4 m long, which will contain 17 one-cell cavities in total. 8 m long drifts have been left for the cryomodules, and 2 m have been left for quadrupoles, correctors, valves, BPMs etc. Figure 8 shows the design of IR10. The redesign of IRs 12, 2 and 4 is in progress, so old versions of these IRs have been included in the lattice and matched. The redesigned versions will be inserted in a future version.

The complete optics for the ring at top energy with two IPs is shown in Fig. 9. The ring has also been matched without squeezing the β-functions at IP8 in order to simulate operation with only one collision point. The key lattice parameters are shown in Table 5. The ring will also need to be matched to the two lower energies.

Table 5: ESR lattice parameters at 17.846 GeV.

Parameter	1 IP	2 IP
Arc-cell phase advance	90°	90°
Emittance (nm)	28	28
Energy spread	0.095%	0.095%
Betatron tunes, Q_x/Q_y	52.12 / 45.10	52.12 / 45.10
Natural chromaticity, ξ_x/ξ_y	-95 / -94	-106 / -110
β_x^*/β_y^* (m)	0.59	0.057

10 Conclusion and outlook

A new version of the ESR lattice has been produced with many changes with respect to the previous version. This new lattice has been given the version number 5.5. The straight sections around IP6 and IP8, which comprise both the spin rotators and the IRs, have been redesigned.

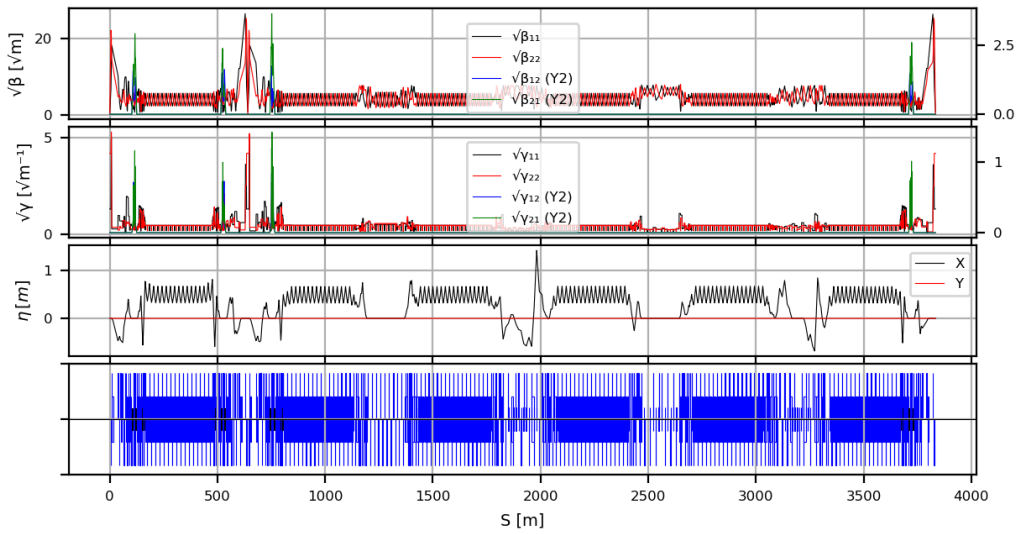


Figure 9: Layout and optics functions for the complete ring with 2 IPs, starting from IP6. The beam travels clockwise around the ring, from left to right in this image.

The geometric layout has been adjusted, and the optics have been rematched. The next steps will be to match the optics for lower beam energies and integrate new versions of IRs 12, 2 and 4.

This new ESR lattice will become the new baseline and will be used for future studies, including polarization and dynamic-aperture optimization. In both these areas there is work to be done in demonstrating feasibility of operation, in particular at top energy.

References

[1] J. Adam et al. *Electron-Ion Collider: Conceptual Design Report*. Brookhaven National Laboratory, Jefferson Lab, 2021. URL: `www.bnl.gov/EC/files/EIC_CDR_Final.pdf`.

[2] D.P. Barber et al. "A solenoid spin rotator for large electron storage rings". In: *Particle Accelerators* 17 (1985), pp. 243–262.

[3] P. Emma. *A spin rotator system for the NLC*. SLAC, 1994.

[4] V. Ptitsin and Yu. Shatunov. "Siberian snakes for electron storage rings". In: *Proc. 17th Particle Accelerator Conf. (PAC'97)* (Vancouver, Canada).

[5] Vladimir N Litvinenko and Alexander A Zholents. *Compensating effect of solenoids with quadrupole lenses*. 2018. arXiv: `1809.11138 [physics.acc-ph]`.